Available online at www.sciencedirect.com
ScienceDirect
Polymer 48 (2007) 7329–7344
polymer
www.elsevier.com/locate/polymer

Pure and mixed gas CH_4 and n-C_4H_{10} permeability and diffusivity in poly(1-trimethylsilyl-1-propyne)

Roy D. Raharjo [a], Benny D. Freeman [a,*], Donald R. Paul [b], Edgar S. Sanders [c]

[a] University of Texas at Austin, Department of Chemical Engineering, Center for Energy and Environmental Resources, 10100 Burnet Road, Building 133, Austin, TX 78758, United States
[b] Department of Chemical Engineering, Texas Materials Institute, University of Texas at Austin, Austin, TX 78712, United States
[c] Air Liquide Research & Development, 200 GBC Drive, Newark, DE 19702, United States

Received 4 September 2007; accepted 17 October 2007
Available online 23 October 2007

Abstract

Pure and mixed gas n-C_4H_{10} and CH_4 permeability coefficients in poly(1-trimethylsilyl-1-propyne) (PTMSP) are reported at temperatures from −20 to 35 °C. CH_4 partial pressures range from 1.1 to 14.6 atm, and n-C_4H_{10} partial pressures range from 0.02 to 1.8 atm. CH_4 permeability decreases with increasing n-C_4H_{10} upstream activity (f/f_{sat}) in the feed. For example, at −20 °C, CH_4 permeability decreases by more than an order of magnitude, from 52,000 to 1700 Barrer, as n-C_4H_{10} activity increases from 0 to 0.73. In contrast, n-C_4H_{10} mixed gas permeability is essentially unaffected by the presence of CH_4. The depression of CH_4 permeability in mixtures is a result of competitive sorption and blocking effects, which reduce both CH_4 mixture solubility and diffusivity, respectively. Diffusion coefficients of n-C_4H_{10} and CH_4 in mixtures were calculated from mixture permeability and mixture solubility data. The CH_4 concentration-averaged diffusion coefficient generally decreases as n-C_4H_{10} activity increases. On the other hand, the n-C_4H_{10} diffusion coefficient is essentially unaffected by the presence of CH_4. Pure and mixed gas activation energies of permeation and diffusion of CH_4 and n-C_4H_{10} are reported. The mixed gas n-C_4H_{10}/CH_4 permeability selectivity increases with increasing n-C_4H_{10} activity and decreasing temperature, and it is higher than pure gas estimates would suggest. Mixture diffusivity selectivity also increases with increasing n-C_4H_{10} activity. The difference between pure and mixed gas permeability selectivity arises from both solubility and diffusivity effects. The dual mode mixed gas permeability model describes the mixture permeability data reasonably well for n-C_4H_{10}. However, the model must be modified to accurately describe the methane data by accounting for the decrease in methane diffusivity due to the presence of n-C_4H_{10} (*i.e.*, blocking). Even though the penetrant concentrations are rather significant at some of the conditions considered, no evidence is observed for phenomena such as multicomponent coupling that would require a model more complex than the binary form of Fick's law. That is, Fick's law in its simplest form adequately describes the experimental data.

Keywords: Mixed gas permeability; Diffusivity; Poly(1-trimethylsilyl-1-propyne) (PTMSP)

1. Introduction

Membrane separation technology has recently emerged as a potential alternative technique to remove higher hydrocarbons from natural gas to reduce the dewpoint and heating value of natural gas to pipeline specifications, prevent condensation during transport, and recover valuable higher hydrocarbons as chemical feedstocks [1]. For economic reasons, membranes for this application should be vapor selective materials such as poly(dimethylsiloxane) (PDMS) or ultra-high free volume polymers such as poly(1-trimethylsilyl-1-propyne) (PTMSP). These polymers, often called solubility selective polymers, are more permeable to larger, more soluble gases than to smaller, less soluble species [2,3]. In this case, methane, the major constituent in natural gas, can be kept at high pressure during the removal of higher hydrocarbons, which avoids the recompression costs

* Corresponding author. Tel.: +1 512 232 2803; fax: +1 512 232 2807.
E-mail address: freeman@che.utexas.edu (B.D. Freeman).

0032-3861/$ - see front matter © 2007 Elsevier Ltd. All rights reserved.
doi:10.1016/j.polymer.2007.10.024

incurred when methane-selective membranes are used for this separation.

Poly(1-trimethylsilyl-1-propyne) (PTMSP) is an extremely permeable glassy polymer with very high vapor/gas selectivities [3,4]. Its oxygen permeability is 9000 Barrer, the highest ever reported [3]. Mixed gas selectivities of organic vapors over permanent gases are as high as 27 for n-C_4H_{10}/CH_4 and 39 for n-C_4H_{10}/H_2 [5]. The rigid double bond in the polymer backbone and the bulky trimethylsilyl side group hinder chain segmental motion and inhibit efficient polymer chain packing, creating large and possibly interconnected free volume elements in the polymer matrix that provide efficient permeation pathways for penetrants. In addition, this very open structure attenuates the polymer's ability to discriminate between large and small penetrant molecules. Thus, unlike conventional glassy polymers, PTMSP sieves penetrant molecules based strongly on their solubility coefficients and therefore, is more permeable to larger, more soluble, higher hydrocarbons than to smaller, less soluble, permanent gases, such as methane.

Although the sorption and transport properties of PTMSP have been reported previously [3,6–9], most studies report only pure gas sorption and transport properties. Mixture properties, which are important for estimating membrane separation performance, are less often reported [4,5]. Rather large differences between pure and mixed gases' permeation properties in PTMSP have been reported [4,5]. For example, Pinnau et al. observed a significant decrease in hydrogen permeability in PTMSP in propane-containing mixtures, which increased the selectivity of propane over hydrogen [5]. Pure hydrogen permeability was 21,000 Barrer, but it decreased to 1100 Barrer in a mixture containing propane at a relative propane pressure (p/p_{sat}) of 0.83 at 25 °C [5]. The propane permeability increased slightly, from 25,000 to 29,000 Barrer, as the relative propane pressure increased from 0 to 0.83 [5]. As a result, the propane/hydrogen selectivity increased from about 1.4, based on pure gas measurements, to approximately 26 in a mixture at high relative propane pressures [5]. In a similar study, Pinnau and Toy reported a considerable increase in n-butane/methane selectivity in PTMSP, from 5 in pure gas to 30 in a mixture of 2 mol% n-butane/methane at 250 psig feed pressure and 23 °C [4]. Under these conditions, methane permeability was only 1800 Barrer, almost 10 times less than the pure gas value (15,400 Barrer) [4]. They suggested that the larger, more soluble, higher hydrocarbon partially blocks the permanent gas permeation pathway, and, therefore, decreases its diffusion coefficient [4,5]. Neither study, however, reported mixture solubility or diffusion data and, in fact, such data are rarely reported in the membrane gas separation literature. This study was motivated, in part, by our desire to understand how much of the reduction in light gas permeability (when co-permeated with more condensable species) was due to reductions in light gas solubility and how much was due to reductions in light gas diffusivity.

This study presents pure and mixed gas n-C_4H_{10}/CH_4 permeability and diffusion coefficients in PTMSP. CH_4 is the primary product in natural gas stream, and n-C_4H_{10} is used as a model marker for higher hydrocarbons in natural gas. The temperatures considered ranged from −20 to 35 °C. The lower limit, −20 °C, is representative of the dewpoint requirement of pipeline-grade natural gas [10]. In addition, conventional processes used to remove higher hydrocarbons (*i.e.*, condensation) operate in this temperature range [10]. The upper limit, 35 °C, is in the range of common operating temperatures for membrane gas separation processes [1]. Results from an earlier companion study of n-C_4H_{10}/CH_4 mixture solubility in PTMSP are used to estimate mixture diffusion coefficients from mixture permeability and solubility data [11]. The present study also quantifies the extent to which deviations between pure and mixed gases' permeation properties in PTMSP depend on differences between pure and mixed gas solubility and diffusivity.

2. Background

The steady state gas permeability coefficient of a polymer membrane is given by [12]:

$$P_A = \frac{N_A l}{f_{A,2} - f_{A,1}} \tag{1}$$

where P_A is the gas permeability coefficient [cm^3(STP) cm/(cm^2 s cmHg)], N_A is the steady state penetrant flux through the membrane [cm^3(STP)/(cm^2 s)], l is the membrane thickness (cm), $f_{A,2}$ is the upstream fugacity, and $f_{A,1}$ is the downstream fugacity. Often, fugacity is replaced by partial pressure in Eq. (1) if the experimental conditions are such that the gas is effectively ideal. In this study, fugacity must be used since gas phase non-idealities are significant in the mixtures considered [13]. If fugacity were not used, then variations in gas permeability, solubility and diffusivity with feed gas composition, temperature, and pressure could be erroneously attributed to issues related to the interaction of the gases with the polymer or with each other inside the polymer rather than to non-idealities only due to gas phase thermodynamic behavior. Thus, the use of fugacity rather than partial pressure is required in this case to clearly separate phenomena due to gas phase non-idealities from actual variations in gas solubility, diffusivity, and permeability in the polymer with composition, pressure, and temperature. The details regarding fugacity calculations are presented elsewhere [13].

Penetrant transport through a polymer film can be modeled using Fick's law. In the simplest case (*i.e.*, one dimension, one penetrant species), the steady state flux is [12]:

$$N_A = -\frac{D_{loc,A}}{1 - w_A}\frac{dC_A}{dx} = -D_A\frac{dC_A}{dx} \tag{2}$$

where C_A is the penetrant concentration, w_A is the penetrant mass fraction in the polymer, x is the spatial coordinate, $D_{loc,A}$ is the binary mutual diffusion coefficient, and D_A is the effective diffusion coefficient in the polymer. More complex models are available to describe penetrant transport in multicomponent mixtures [14]; however, in this work, the form of Fick's law given in Eq. (2) was found to be adequate to describe the mixture transport data once proper accounting

was made for the influence of each component on the other's solubility and diffusivity using the dual mode framework.

Combining Eqs. (1) and (2) and integrating across the film thickness yields [12]:

$$P_A = \frac{1}{f_{A,2} - f_{A,1}} \int_{C_{A,1}}^{C_{A,2}} D_A \, dC_A \tag{3}$$

where $C_{A,2}$ and $C_{A,1}$ are the penetrant concentrations at the upstream and downstream faces, respectively, of the polymer membrane. Eq. (3) can also be written as [12]:

$$P_A = \overline{D}_A \cdot \left(\frac{C_{A,2} - C_{A,1}}{f_{A,2} - f_{A,1}} \right) \tag{4}$$

where $\overline{D}_A$ is the concentration-averaged effective diffusion coefficient defined as follows:

$$\overline{D}_A = \frac{1}{C_{A,2} - C_{A,1}} \int_{C_{A,1}}^{C_{A,2}} D_A \, dC_A \tag{5}$$

when the downstream fugacity is much less than the upstream fugacity (*i.e.*, $C_{A,2} >> C_{A,1}$ and $f_{A,2} >> f_{A,1}$), Eq. (4) can be simplified as follows:

$$P_A = \overline{D}_A \cdot S_A \tag{6}$$

where S_A is the solubility coefficient of A evaluated at the upstream face of the membrane: $S_A = C_{A,2}/f_{A,2}$.

The selectivity of a polymer for penetrant A relative to penetrant B is the ratio of the permeability coefficients of the two penetrants [12]:

$$\alpha_{A/B} = \frac{P_A}{P_B} = \left[\frac{\overline{D}_A}{\overline{D}_B} \right] \left[\frac{S_A}{S_B} \right] \tag{7}$$

where $\overline{D}_A/\overline{D}_B$ is the diffusivity selectivity, and S_A/S_B is the solubility selectivity. Diffusivity selectivity is strongly influenced by the size difference between A and B and by the size-sieving ability of the polymer matrix [15]. Solubility selectivity is controlled by the relative penetrant condensability and the affinity between the penetrants and the polymer matrix [15]. In a weakly size-sieving polymer such as PTMSP, the overall selectivity depends significantly on solubility selectivity. Note that since permeability is defined based on fugacity rather than partial pressure, this definition of selectivity will not be equal to the ratios of the mole fractions of A and B in the permeate and retentate, which is the definition of selectivity in conventional separation processes [12].

Gas permeability in glassy polymers is often described using the dual mode transport model. The pure gas permeability at negligible downstream fugacity can be written as follows [16]:

$$P_A = k_{D_A} \overline{D}_{D_A} + \frac{C'_{H_A} b_A \overline{D}_{H_A}}{1 + b_A f_{A,2}} \tag{8}$$

where $\overline{D}_{D_A}$ is the average effective diffusion coefficient of penetrant molecules in the Henry's law region, and $\overline{D}_{H_A}$ is the average effective diffusion coefficient in the nonequilibrium excess volume or Langmuir region. k_{D_A}, C'_{H_A}, and b_A are the Henry's law constant, the Langmuir sorption capacity, and the Langmuir affinity parameters, respectively, which are determined from sorption measurements [11]. At infinite dilution, the pure gas permeability in Eq. (8) can be expressed as:

$$P_o = \lim_{f_{A,2} \to 0} P_A = k_{D_A} \overline{D}_{D_A} + C'_{H_A} b_A \overline{D}_{H_A} \tag{9}$$

Koros et al. [16] extended the dual mode transport model to mixtures by introducing competitive sorption effects into Eq. (8). The mixed gas permeability of component A in the presence of component B in a mixture is written as follows [16]:

$$P_A = k_{D_A} \overline{D}_{D_A} + \frac{C'_{H_A} b_A \overline{D}_{H_A}}{1 + b_A f_{A,2} + b_B f_{B,2}} \tag{10}$$

where b_B and $f_{B,2}$ are the Langmuir affinity parameter of component B and the upstream fugacity of B, respectively. A similar expression for the permeability of component B in the mixture can be derived in terms of its sorption and transport parameters [16]:

$$P_B = k_{D_B} \overline{D}_{D_B} + \frac{C'_{H_B} b_B \overline{D}_{H_B}}{1 + b_A f_{A,2} + b_B f_{B,2}} \tag{11}$$

The temperature dependence of permeability, diffusivity, and solubility at temperatures far removed from polymer thermal transitions is usually described as follows [15]:

$$P_A = P_o \exp\left(\frac{-E_P}{RT} \right) \tag{12}$$

$$S_A = S_o \exp\left(\frac{-\Delta H_S}{RT} \right) \tag{13}$$

$$\overline{D}_A = D_o \exp\left(\frac{-E_D}{RT} \right) \tag{14}$$

where P_o, S_o, and D_o are pre-exponential factors, R is the universal gas constant, T is the absolute temperature, and E_P, ΔH_S, and E_D are the activation energy of permeation, the enthalpy of sorption, and the activation energy of diffusion, respectively. Combining Eqs. (6) and (12–14) yields the following expression:

$$E_P = E_D + \Delta H_S \tag{15}$$

This formalism is straightforward and self-consistent when permeability, solubility, and diffusivity are independent of pressure. If this is not the case, then care must be exercised in applying this model [17].

3. Experimental

3.1. Materials

Poly(1-trimethylsilyl-1-propyne) (PTMSP) was kindly supplied by Air Products, Inc. (St. Louis, MO). Dense films of PTMSP were prepared by casting a polymer solution, prepared from a 2 wt% PTMSP in toluene, into a flat-bottomed glass dish at ambient conditions. After drying, samples were stored in liquid methanol at ambient conditions to inhibit physical aging and help alleviate sample-to-sample property differences due to minor variations in thermal processing history [18]. The films were removed from methanol and dried at ambient conditions for 24 h before using them in permeation experiments. Film thicknesses were determined with a digital micrometer (Mitutoyo) readable to ±1 μm. Samples for the permeability measurements were approximately 250 μm thick. The density of the PTMSP films at 25 °C was approximately 0.73 ± 0.01 g/cm^3, determined by measuring the difference in film weights in water and in air.

Chemical-grade CH_4 and n-C_4H_{10} (99% purity) were purchased from Air Gas Southwest Inc. (Corpus Christi, TX). Certified 2, 4, 6, and 8 mol% n-C_4H_{10}/CH_4 were purchased from Air Liquide America Corporation (Houston, TX). All gases were used as-received.

3.2. Permeability measurements

The CH_4 and n-C_4H_{10} pure and mixed gases' permeabilities were measured using a constant pressure/variable volume apparatus as described previously [19–21]. A mass flow controller (MKS Model# 1179A23CSIBV, Wilmington, MA) was installed on the upstream side to regulate residue flow rate. Helium was used to sweep the downstream side of the membrane and carry the permeate (*i.e.*, CH_4 and n-C_4H_{10}) to a gas chromatograph (GC). The total flow rate on the downstream side (*i.e.*, helium + permeate) was measured with a soap film flow meter. The measurement temperatures ranged from −20 to 35 °C. A constant temperature circulator regulated the system temperature to ±0.1 °C.

For pure gas permeability measurements, the feed pressures were varied from 4.4 to 14.6 atm and from 1.2 to 1.8 atm, for CH_4 and n-C_4H_{10}, respectively. The n-C_4H_{10} pure gas permeability in PTMSP was determined at 25 and 35 °C. The permeation apparatus permits measurement only at total upstream pressures greater than atmospheric pressure. Pure gas n-C_4H_{10} permeability coefficients in PTMSP at low temperatures (*e.g.*, 0 and −20 °C) could not be measured, since the saturation pressure of n-C_4H_{10} was lower than 1 atm [22]. A constant residue flow rate of 20 cm^3/min was maintained during the pure gas permeability measurement to remove any helium that might permeate from the downstream to the upstream side of the film.

In the mixture measurements, sufficient residue flow rate was maintained (*i.e.*, a stage cut of less than 1%) to prevent concentration polarization: that is, the residue flow rate was set high enough to ensure that the results were independent of residue flow rate. The feed pressure was varied from 1.1 to 14.6 atm. The partial pressure of CH_4 and n-C_4H_{10} on the downstream side of the film was maintained at practically zero (<0.05 atm) by adjusting the helium flow rate. In this way, the downstream n-C_4H_{10} activity, defined as the ratio of fugacity to the saturation fugacity at a given temperature (f/f_{sat}), was always less than 0.01. The saturation fugacity was the fugacity at the saturation pressure (p_{sat}), which was estimated using the Wagner equation [22].

The steady state gas permeability was calculated as follows:

$$P_A = \frac{l}{f_{A,2} - f_{A,1}} \frac{273}{TA} \frac{p_{atm}}{76} \left(y_{A,1} \frac{dV}{dt} \right) \tag{16}$$

where $f_{A,2}$ and $f_{A,1}$ are the upstream and downstream fugacities of gas A, respectively. These fugacities were determined as described previously [13]. $y_{A,1}$ is the mole fraction of gas A on the downstream side of the film determined using the GC, p_{atm} is the atmospheric pressure, A is the film area (cm^2), T is temperature (K), l is film thickness (cm), and dV/dt is the steady state volumetric displacement rate of a soap film in the bubble flow meter connected to the permeate exhaust from the permeation cell (cm^3/s).

The pure and mixed gas permeability measurements for each sample (*i.e.*, fresh) were completed in 8 h at most. The pure gas CH_4 and n-C_4H_{10} permeabilities in PTMSP were essentially constant over this time period, indicating that the physical aging of the film was minimal during the time of measurement. The pure gas CH_4 permeability decreased after exposing the film to n-C_4H_{10} (*i.e.*, after mixture measurements). For example, the pure gas CH_4 permeability at 4.4 atm feed pressure and 35 °C decreased by approximately 22%, from 24,000 to 19,000 Barrer, after exposing the film to a 2 mol% n-C_4H_{10}/CH_4 mixture up to 14.6 atm. This behavior can be related to penetrant-induced hysteresis, which has been observed previously in another high free volume glassy polymer [23]. To avoid such hysteresis effect, fresh PTMSP films were used for each mixture permeability measurement.

4. Results and discussion

4.1. Pure gas permeability

Fig. 1(a) and (b) presents CH_4 and n-C_4H_{10} pure gas permeability coefficients in PTMSP as a function of upstream fugacity, or upstream activity for n-C_4H_{10}, at temperatures from −20 to 35 °C. In general, CH_4 and n-C_4H_{10} permeabilities decrease with increasing upstream fugacity and temperature. The infinite dilution permeability values at each temperature are calculated using Eq. (9) and presented in Table 1. The CH_4 and n-C_4H_{10} permeability values are somewhat higher than some reported literature values for PTMSP [3,4,9]. Merkel et al. reported CH_4 pure gas infinite dilution permeability of 15,000 Barrer at 35 °C [3]. Srinivasan et al. reported a value of 17,000 Barrer at 25 °C [9]. For comparison, the CH_4 pure gas infinite dilution permeability coefficients in this study are 28,000 and

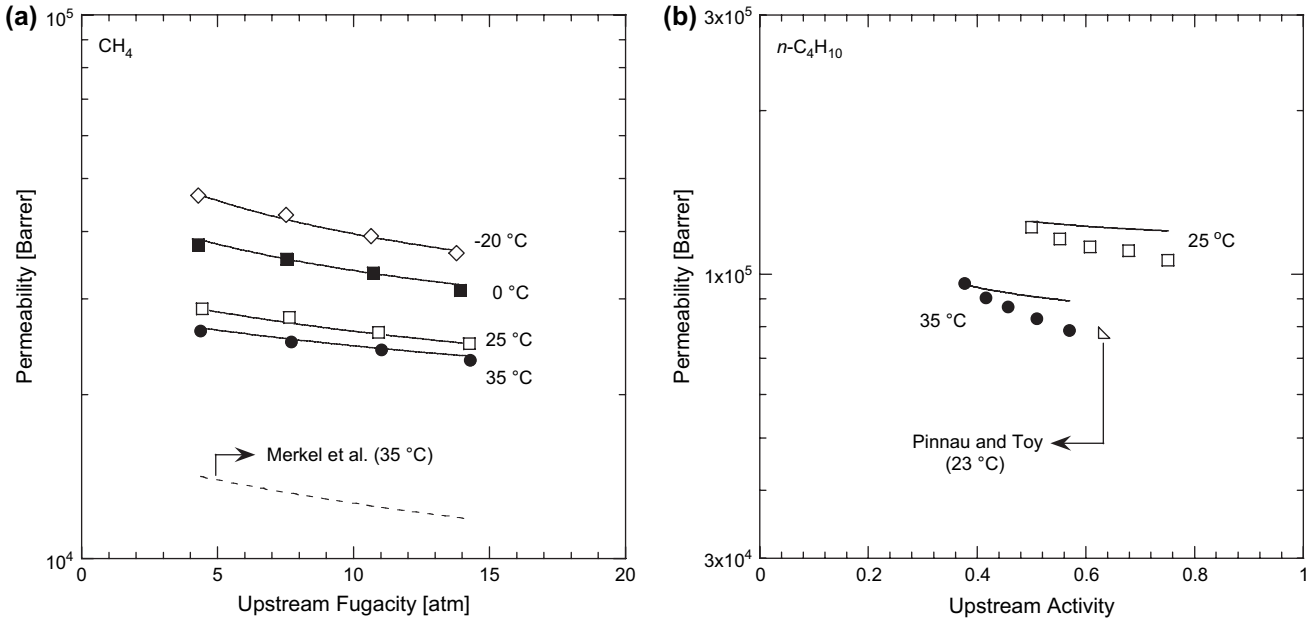

Fig. 1. (a) Pure gas permeability of CH_4 in PTMSP as a function of upstream fugacity and temperature. The dashed line represents pure CH_4 permeability values at 35 °C reported by Merkel et al. [3]. (b) Pure gas permeability of n-C_4H_{10} in PTMSP as a function of upstream fugacity and temperature. The solid lines represent a nonlinear least squares fit of Eq. (8) to the experimental data. The pure gas n-C_4H_{10} permeability value in PTMSP reported by Pinnau and Toy [4] is presented as a reference.

Table 1
Dual mode diffusion coefficients, permeability and concentration-averaged diffusion coefficients at infinite dilution in PTMSP

T (°C)	CH_4[a]				n-C_4H_{10}[b]			
	$\overline{D}_D \times 10^6$ (cm^2/s)	$\overline{D}_H \times 10^6$ (cm^2/s)	$\overline{D}_o \times 10^6$ (cm^2/s)	$P_o \times 10^{-3}$ (Barrer)	$\overline{D}_D \times 10^6$ (cm^2/s)	$\overline{D}_H \times 10^6$ (cm^2/s)	$\overline{D}_o \times 10^6$ (cm^2/s)	$P_o \times 10^{-3}$ (Barrer)
−20	180 ± 20	28 ± 3	44 ± 4	52 ± 3	9 ± 1	1.6 ± 0.2	1.7 ± 0.2	2300 ± 150
0	200 ± 20	29 ± 3	52 ± 5	41 ± 2	14 ± 1	2.3 ± 0.2	2.5 ± 0.2	1400 ± 80
25	180 ± 20	35 ± 3	61 ± 6	31 ± 2	21 ± 2	3.3 ± 0.3	3.8 ± 0.3	580 ± 40
35	200 ± 20	39 ± 4	70 ± 7	28 ± 2	20 ± 2	4.4 ± 0.4	5.1 ± 0.5	450 ± 30

1 Barrer = 1×10^{-10} cm^3(STP) cm/(cm^2 s cmHg).
[a] Based on pure gas measurements.
[b] Based on pure and mixed gas measurements.

31,000 Barrer at 35 and 25 °C, respectively. Pinnau and Toy reported n-C_4H_{10} permeability of 78,000 Barrer at 23 °C and 0.63 n-C_4H_{10} upstream activity (p/p_{sat}), about 30% lower than the value determined in this study under similar upstream conditions (112,000 Barrer at 25 °C and 0.61 n-C_4H_{10} upstream activity). Gas transport properties in PTMSP are quite sensitive to film preparation conditions and processing history [24,25]. As a result, PTMSP permeability values in the literature vary widely [9]. Our PTMSP film density (0.73 g/cm^3) is slightly lower than that reported by Merkel et al., Srinivasan et al., and Pinnau and Toy (0.75 g/cm^3) [3,4,9], and this lower density translates to a higher fractional free volume (FFV), which may explain the higher permeability values in this study. Recently, Hu et al. reported CH_4 permeability at 25 °C to be 30,000 Barrer in PTMSP, which is quite similar to our value [26]. However, n-C_4H_{10} permeability and polymer density were not reported in this study, so one cannot comment further on the reason for the good agreement between our CH_4 permeability and theirs.

4.2. Pure gas diffusivity

Concentration-averaged diffusion coefficients were estimated from the permeability and sorption data using the following rearranged form of Eq. (6) [12]:

$$\overline{D}_A = P_A\left(\frac{f_{A,2}}{C_{A,2}}\right) \tag{17}$$

Fig. 2(a) and (b) presents pure gas CH_4 and n-C_4H_{10} concentration-averaged diffusion coefficients in PTMSP as a function of upstream fugacity, or upstream activity for n-C_4H_{10}. The pure gas diffusion coefficient of CH_4 increases with increasing upstream fugacity and temperature, consistent with the results of Merkel et al. [3], although our values are somewhat higher than theirs, consistent with the higher permeability coefficients reported in Fig. 1. Merkel et al. reported that the pure gas CH_4 diffusion coefficient at 35 °C and infinite dilution was 3.6×10^{-6} cm^2/s [3]. As discussed earlier, this discrepancy is most likely due to the lower film density in our study.

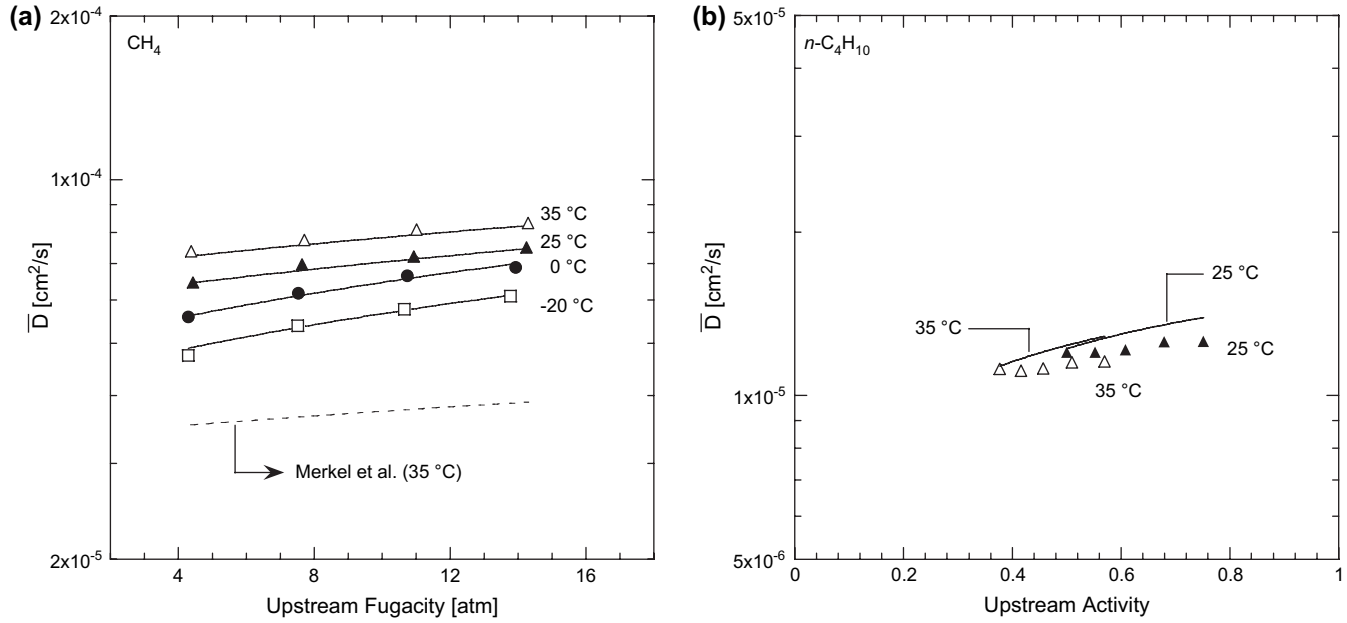

Fig. 2. (a) Effect of upstream fugacity and temperature on pure gas CH_4 concentration-averaged diffusion coefficients in PTMSP. The dashed lines are pure gas values at 35 °C determined by Merkel et al. [3]. (b) Pure gas n-C_4H_{10} concentration-averaged diffusion coefficients in PTMSP as a function of upstream activity and temperature. The solid lines represent Eqs. (22) and (23) using parameters in Table 1.

The diffusion coefficients in PTMSP are about 10^3–10^6 times higher than those observed in conventional, low free volume, glassy polymers (*e.g.*, polycarbonate) [27].

4.3. Mixed gas permeability

Fig. 3(a) presents CH_4 mixed gas permeability in PTMSP as a function of n-C_4H_{10} feed fugacity. The presence of n-C_4H_{10} significantly decreases CH_4 mixture permeability in PTMSP. For example, at 35 °C, CH_4 permeability decreases by more than a factor of 10, from 28,000 in pure gas at infinite dilution, to 2200 Barrer in the presence of 0.77 atm n-C_4H_{10} fugacity (~0.26 n-C_4H_{10} activity). At −20 °C, CH_4 permeability decreases from 52,000 in pure gas at infinite dilution, to 1700 Barrer in the presence of 0.32 atm n-C_4H_{10} fugacity (~0.73 n-C_4H_{10} activity), a more than 30-fold decrease. The

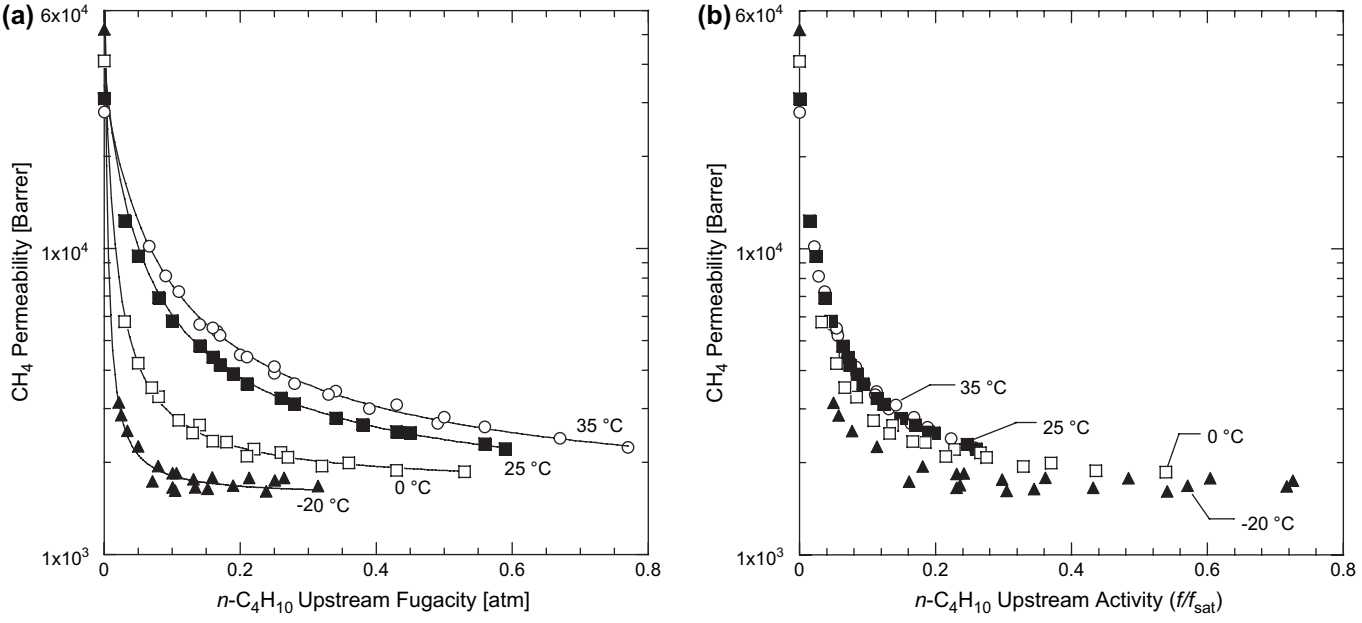

Fig. 3. CH_4 permeability in PTMSP as a function of (a) n-C_4H_{10} upstream fugacity and (b) n-C_4H_{10} upstream activity in the feed at 35 °C (○), 25 °C (■), 0 °C (□), and −20 °C (▲). The feed gas compositions are 2, 4, 6, and 8 mol% n-C_4H_{10} in CH_4. The total feed pressure was from 1.1 to 14.6 atm. The permeate was swept with helium at 1 atm, so the permeate partial pressures of CH_4 and n-C_4H_{10} were negligible. The lines represent model fits to the experimental data using Eq. (27) and the parameters in Table 2.

CH_4 mixture permeability data at various temperatures collapse slightly when plotted as a function of n-C_4H_{10} upstream activity, rather than fugacity, as shown in Fig. 3(b). The CH_4 permeability appears to approach a plateau value at high n-C_4H_{10} upstream activity.

As will be described in more detail later, this decrease in mixture CH_4 permeability is partly due to the decrease in the CH_4 solubility coefficient in the mixtures due to competitive sorption effects [11]. n-C_4H_{10}, which is much more condensable than CH_4, preferentially occupies the Langmuir sorption sites, thereby reducing CH_4 sorption capacity in this region, which decreases CH_4 solubility in the polymer [11]. Additionally, the reduction in the CH_4 diffusion coefficient in mixtures due to n-C_4H_{10} blocking effects also contributes to the decrease in CH_4 mixture permeability in PTMSP.

The presence of CH_4 does not noticeably change n-C_4H_{10} permeability in PTMSP. Fig. 4 presents n-C_4H_{10} permeability in PTMSP as a function of n-C_4H_{10} feed activity for pure gas and mixed gas conditions. The n-C_4H_{10} permeability coefficients decrease with increasing n-C_4H_{10} activity, which is qualitatively consistent with expectations of the dual mode model (*i.e.*, Eq. (8)). The pure gas data agree with the mixture permeability data, suggesting that n-C_4H_{10} permeation is not influenced by the presence of CH_4.

The temperature dependence of gas permeability in pure gas and mixtures can be described using Eq. (12) provided one restricts its use to a given upstream gas concentration. In this case, the activation energy of permeation, E_P, at a fixed penetrant concentration in the polymer can be calculated as follows [21]:

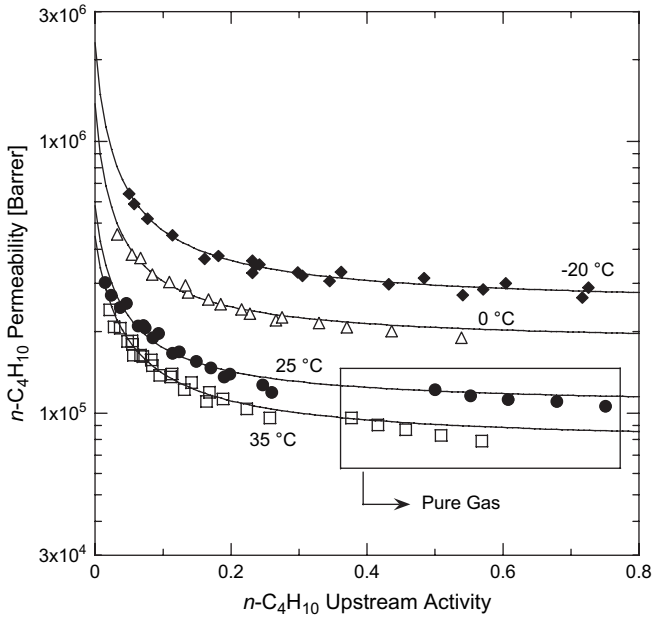

Fig. 4. n-C_4H_{10} permeability in PTMSP as a function of n-C_4H_{10} upstream activity. The feed gas compositions are 2, 4, 6, and 8 mol% n-C_4H_{10} in CH_4. The total feed pressure was from 1.1 to 14.6 atm. The permeate was swept with helium at 1 atm, so the permeate partial pressures of CH_4 and n-C_4H_{10} were negligible. The lines represent model fits to the experimental data using Eq. (10) and the parameters in Table 1. For comparison, pure gas n-C_4H_{10} permeation data are also presented.

Table 2
CH_4 dual mode diffusion coefficient parameters based on Eq. (27) using pure and mixed gas data

T (°C)	$\overline{D}_D \times 10^6$ (cm^2/s)	$\overline{D}_{Ho} \times 10^6$ (cm^2/s)	α_H
−20	12 ± 1	63 ± 7	0.11 ± 0.01
0	15 ± 1	74 ± 8	0.077 ± 0.008
25	16 ± 2	86 ± 6	0.055 ± 0.006
35	18 ± 2	98 ± 7	0.058 ± 0.006

$$E_P^C = -R\left(\frac{d\ln P_A}{d1/T}\right)_C \tag{18}$$

where E_P^C is the activation energy of permeation at fixed gas concentration C, which is taken, in this study to refer to a fixed gas concentration at the upstream face of the film. The permeability coefficients are estimated from the dual mode permeability models (*i.e.*, Eqs. (10) and (27)) using parameters determined based on experimental data (Tables 1 and 2). The upstream gas concentrations were calculated using the dual mode sorption model [11].

Fig. 5 presents pure and mixed gas E_P^C values for CH_4 and n-C_4H_{10}. The CH_4 pure gas E_P^C values (open symbols) are presented as a function of upstream CH_4 concentration. The error bars are determined using the propagation of errors method [28]. These pure gas E_P^C values for CH_4 in PTMSP are negative (*i.e.*, exothermic), which is unusual for permanent gas permeation in polymers [15]. That is, CH_4 permeability in PTMSP increases with decreasing temperature. The pure gas E_P^C of CH_4 in

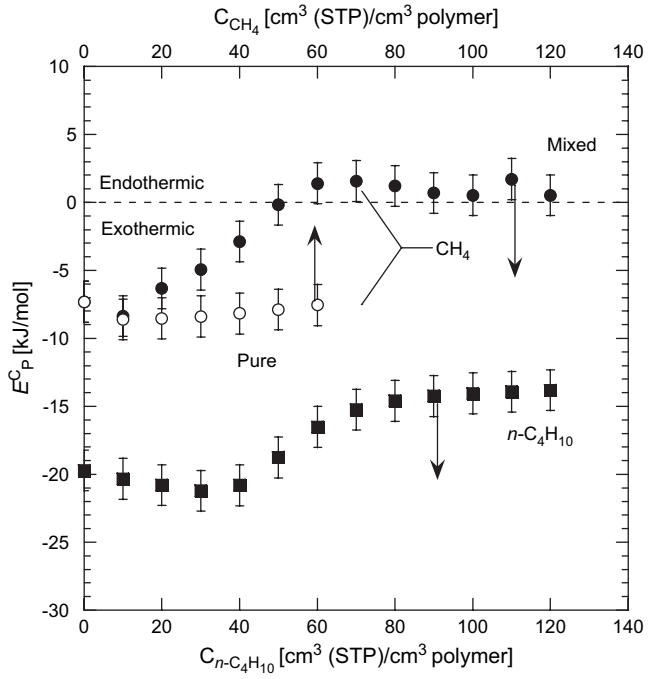

Fig. 5. Activation energies of permeation of CH_4 and n-C_4H_{10} as a function of penetrant concentration at the upstream face of the film. The n-C_4H_{10} activation energies of permeation are estimated based on mixed gas data, while both pure and mixed gas estimates of the CH_4 activation energies are provided. There is essentially no difference between the pure and mixed gas n-C_4H_{10} permeability data in PTMSP, so the activation energies of permeation for n-C_4H_{10} are the same, within the uncertainty in the measurements, in both pure and mixed gas.

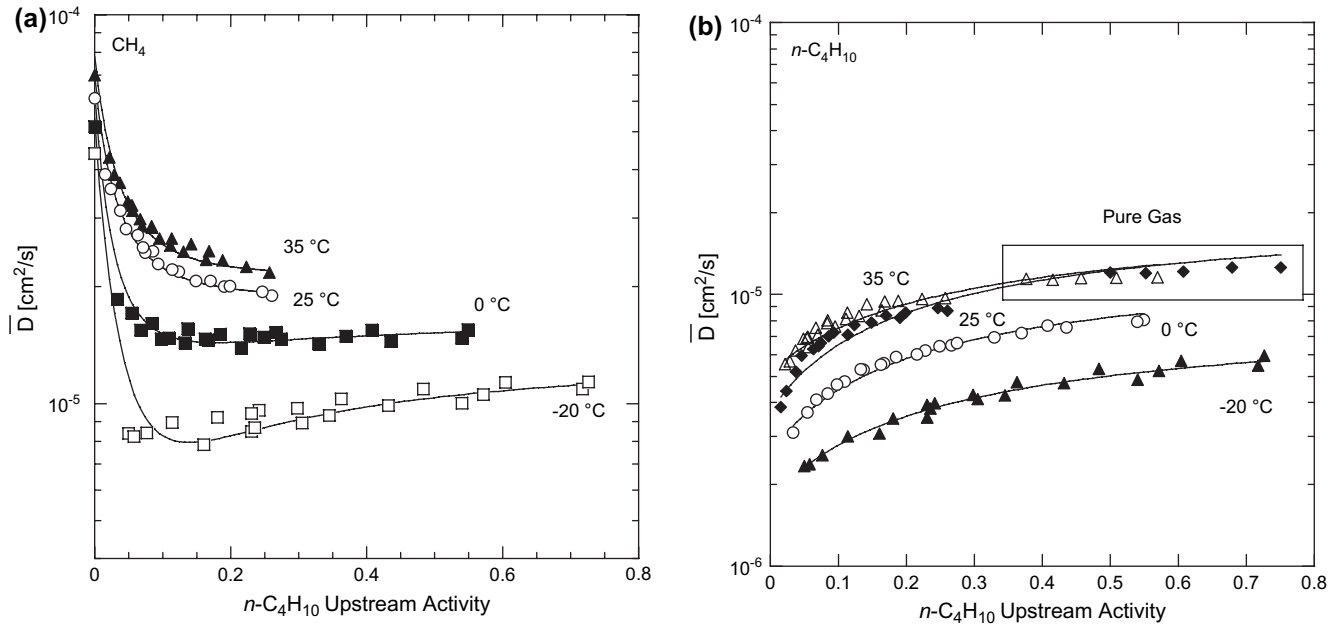

Fig. 6. The average effective diffusion coefficient of: (a) CH_4 and (b) n-C_4H_{10} as a function of n-C_4H_{10} activity in the feed mixtures. The solid lines in (a) are predictions from Eq. (28) using the parameters in Table 2. The lines in (b) are predictions from Eq. (23) using the parameters in Table 1.

PTMSP (*i.e.*, at infinite dilution) is -7.3 ± 1.5 kJ/mol, which is consistent with literature values of -6.3 and -7.6 kJ/mol reported by Masuda et al. [29] and Merkel et al. [30], respectively. In conventional glassy and even rubbery polymers, E_P^C values for permanent gases (*e.g.*, H_2, N_2, CH_4) are usually positive [15]. Negative E_P^C values for such light gases are commonly observed for microporous solids in which the pore dimensions are larger than the kinetic diameter of the diffusing gas molecules [9]. In contrast to the pure gas behavior, where E_P^C of CH_4 is practically independent of concentration, the E_P^C for CH_4 in n-C_4H_{10}/CH_4 mixtures initially increases, from -7.3 ± 1.5 for pure gas, with increasing n-C_4H_{10} concentration before reaching a plateau, at approximately 1.1 ± 1.5 kJ/mol, at higher n-C_4H_{10} concentrations, as shown in Fig. 5. The increase in the E_P^C of CH_4 with increasing n-C_4H_{10} concentration is presumably related to the combination of blocking and competitive sorption effects [11], which reduce CH_4 diffusivity and solubility, respectively, in mixtures with n-C_4H_{10}. Positive E_P^C values are typical for permanent gas permeation in conventional glassy and rubbery polymers [15]. For example, the E_P^C of pure gas CH_4 in poly(vinyl chloride) (PVC), a glassy polymer, is 66.2 kJ/mol [31]. The E_P^C of CH_4 in rubbery PDMS is 6.8 kJ/mol in the pure gas case and 5.1 kJ/mol in the presence of 60 cm^3(STP)/cm^3 of n-C_4H_{10} at the upstream face of the film [21]. The pure and mixed gas E_P^C values of n-C_4H_{10} with n-C_4H_{10} concentration qualitatively exhibit a trend similar to that of CH_4 in gas mixtures. At n-C_4H_{10} concentrations greater than 40 cm^3(STP)/cm^3, the E_P^C of n-C_4H_{10} increases with increasing n-C_4H_{10} concentration until it reaches a plateau at approximately -13.9 ± 1.5 kJ/mol. Because n-C_4H_{10} permeability coefficients are not affected by the presence of CH_4, the E_P^C values for n-C_4H_{10} are the same in both pure and mixed gas cases.

4.4. Mixed gas diffusivity

The concentration-averaged CH_4 and n-C_4H_{10} diffusion coefficients in mixtures were estimated using Eq. (17) and are presented in Fig. 6(a) and (b), respectively. The presence of n-C_4H_{10} considerably reduces the CH_4 diffusion coefficient in the polymer even at low levels of n-C_4H_{10} sorption. For example, at 35 °C, the CH_4 diffusion coefficient decreases more than 70%, from 7.0×10^{-5} in pure gas at infinite dilution (the point at an n-C_4H_{10} activity of zero in Fig. 6(a)), to 2.0×10^{-5} cm^2/s when the upstream n-C_4H_{10} activity is 0.20. In contrast, n-C_4H_{10} diffusion coefficients increase with increasing n-C_4H_{10} activity (*cf.*, Fig. 6(b)). For n-C_4H_{10}, there is no measurable difference between pure and mixed gas diffusivity values; that is, the effect of CH_4 on n-C_4H_{10} diffusion coefficients is negligible.

The blocking effect, which acts to reduce CH_4 diffusivity due to the presence of n-C_4H_{10}, and the competitive sorption effect, which acts to reduce CH_4 solubility due to the presence of n-C_4H_{10} [11], are both responsible for the mixed gas permeability depression in Fig. 3(a). Fig. 7(a) and (b) presents the ratio of CH_4 mixed gas permeability, solubility, and diffusivity to those of pure gas at infinite dilution as a function of n-C_4H_{10} activity at 35 and -20 °C. The CH_4 permeability decrease in the mixture is substantial: at -20 °C and 0.73 n-C_4H_{10} activity, the mixed gas CH_4 permeability in PTMSP is only 3.3% of the pure gas value. Both solubility and diffusivity contribute to this reduction, with solubility reduction (*i.e.*, competitive sorption) generally contributing somewhat more to the overall permeability reduction than diffusivity reduction. The ratio of CH_4 mixed gas permeability, solubility, and diffusivity to those of pure gas at infinite dilution at other temperatures (*i.e.*, 25 and 0 °C) is presented in Supplementary section.

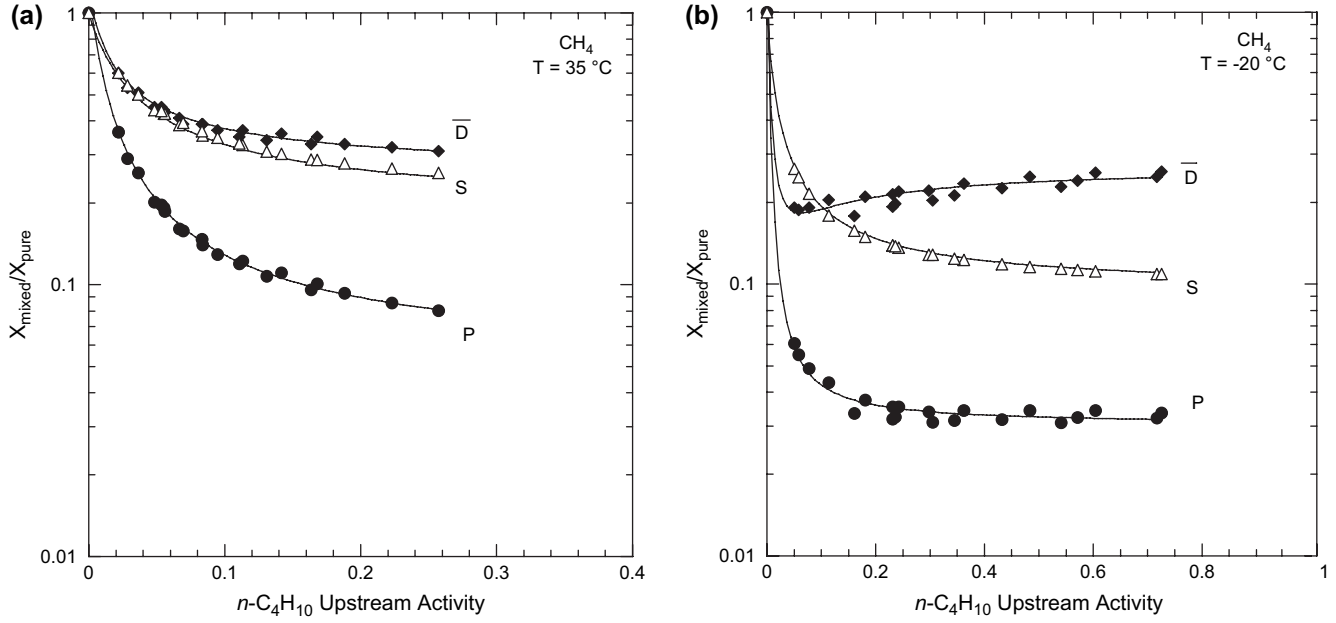

Fig. 7. The ratio of CH_4 mixed gas permeability (P), solubility (S), and diffusivity ($\overline{D}$) coefficients to those of pure gas at infinite dilution as a function of n-C_4H_{10} activity at (a) 35 °C and (b) −20 °C. The total feed pressure was from 1.1 to 14.6 atm. The solid lines are predictions of the dual mode models (*i.e.*, Eqs. (8), (27), (22), (28), and Ref. [11]).

The local effective diffusion coefficient, D_A, characterizes the ability of a penetrant to migrate through a polymer at a particular, well-defined penetrant concentration [32]. Pure gas D_A values were calculated from the slope of the sorption isotherm [11] and the pressure dependence of permeability as follows [33]:

$$D_A(C_{A,2}) = \left[P_A + f_{A,2}\frac{dP_A}{df_{A,2}}\right]_{f_{A,2}}\left(\frac{df_A}{dC_A}\right)_{f_{A,2}} \quad (19)$$

The local effective diffusion coefficients of n-C_4H_{10} in n-C_4H_{10}/CH_4 mixtures are also calculated using Eq. (19) because n-C_4H_{10} permeability, diffusivity, and solubility in these mixtures are essentially unaffected by the presence of CH_4. In Eq. (19), $dP_A/df_{A,2}$ is estimated from the measured n-C_4H_{10} fugacity dependence of n-C_4H_{10} mixture permeability in the polymer, and df_A/dC_A is estimated from the pure gas sorption isotherms of n-C_4H_{10} in PTMSP [11]. Fig. 8(a) presents D_A values for n-C_4H_{10} in the mixture as a function of n-C_4H_{10} concentration. The n-C_4H_{10} diffusion coefficients increase with increasing n-C_4H_{10} concentration, similar to the trend presented in Fig. 6(b). At sufficiently high n-C_4H_{10} concentration, the n-C_4H_{10} diffusion coefficient reaches a plateau and no longer changes with n-C_4H_{10} concentration in the polymer.

The local effective diffusion coefficients of CH_4 in mixtures, which depend on n-C_4H_{10} concentration in the polymer, was estimated as follows [21]:

$$D_B(C_{A,2}) = \frac{D_A(C_{A,2})}{\left[\frac{d}{dC_A}\left[\frac{P_A f_{A,2} S_B}{P_B}\right]\right]_{f_{A,2}}} \quad (20)$$

where the subscripts A and B refer to n-C_4H_{10} and CH_4, respectively. D_A was determined using Eq. (19). A different formula (Eq. (20) instead of Eq. (19)) is used to calculate the local effective diffusion coefficients of CH_4 in mixtures because these values depend sensitively on n-C_4H_{10} concentration. Fig. 8(b) presents the local effective diffusion coefficients of CH_4 in mixtures (*i.e.*, D_B) as a function of n-C_4H_{10} concentration at the upstream side of the membrane. There is a minimum in the local CH_4 diffusion coefficient with concentration that was not apparent previously in Fig. 6(a). For example, at 35 °C, the CH_4 local effective diffusion coefficient initially decreases with increasing n-C_4H_{10} concentration, from 7.0×10^{-5} in pure gas (infinite dilution) to a minimum value of approximately 1.5×10^{-5} cm^2/s in the presence of 32 cm^3(STP) n-C_4H_{10}/cm^3 polymer. At higher n-C_4H_{10} concentrations, the CH_4 local diffusion coefficients increase, reaching a value of 2.2×10^{-5} cm^2/s in the presence of 58 cm^3(STP) n-C_4H_{10}/cm^3 polymer. This trend can perhaps be rationalized by a competition between two phenomena: (1) blocking of the large, interconnected free volume elements in PTMSP by n-C_4H_{10}, which hinders CH_4 transport, and (2) plasticization of the film by n-C_4H_{10} sorption, which increases the CH_4 diffusion coefficient. At low n-C_4H_{10} concentration, n-C_4H_{10} sorption occurs predominantly in the Langmuir regions [11], with little or no plasticization. Thus, the blocking effect is stronger than the plasticization effect at lower n-C_4H_{10} concentrations. As a result, CH_4 diffusion coefficients initially decrease with increasing n-C_4H_{10} concentration. As n-C_4H_{10} concentration increases, the Langmuir region becomes progressively more saturated, resulting in a greater fraction of n-C_4H_{10} sorption in the Henry's law region [11], rendering plasticization more important. In addition, the blocking effect should reach a maximum, hypothetically, as

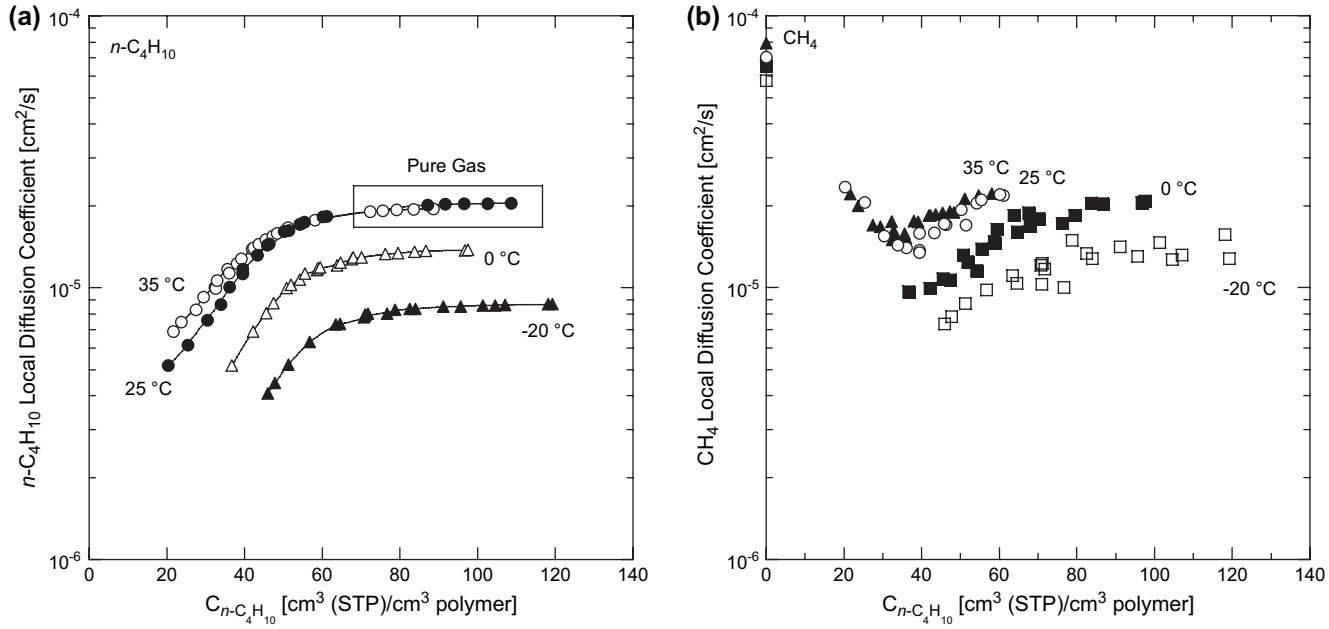

Fig. 8. Local diffusion coefficients as a function of n-C_4H_{10} concentration in the polymer: (a) n-C_4H_{10} and (b) CH_4. For comparison, pure gas n-C_4H_{10} data (*i.e.*, the data points in the box) are presented along with the mixed gas data. The solid lines in (a) are predictions of the dual mode permeability model (*i.e.*, Eq. (24)). The pure gas CH_4 local diffusion coefficients are reported at 4.4 atm upstream pressure.

the Langmuir region becomes saturated. At higher n-C_4H_{10} concentrations, plasticization overcomes the blocking effect, and, consequently, the CH_4 diffusion coefficient increases with increasing n-C_4H_{10} concentration.

Throughout this study, the magnitude of the CH_4 diffusion coefficient *reduction* due to blocking effect is considerably greater than the CH_4 diffusion coefficient *enhancement* due to the plasticization effect, as shown in Fig. 8(b). For example, at 25 °C, the blocking effect decreases the CH_4 local effective diffusion coefficient by a factor of five, from 6.1×10^{-5} in pure gas (infinite dilution) to 1.3×10^{-5} cm^2/s in the presence of 39 cm^3(STP) n-C_4H_{10}/cm^3 polymer. In contrast, the plasticization effect increases the CH_4 local diffusion coefficient by a factor of only approximately two, from 1.3×10^{-5} to 2.2×10^{-5} cm^2/s, as n-C_4H_{10} concentration goes from 39 to 60 cm^3(STP)/cm^3.

The temperature dependence of gas diffusivity in pure gas and mixtures can be characterized using Eq. (14). The activation energy of diffusion, E_D, at a fixed penetrant concentration can be determined as follows [21]:

$$E_D^C = -R\left(\frac{\mathrm{d}\ln \overline{D}_A}{\mathrm{d}1/T}\right)_C \tag{21}$$

where E_D^C is the activation energy of diffusion when the penetrant concentration is C. Fig. 9 shows that although E_D^C for pure CH_4 is not a strong function of concentration, the E_D^C of CH_4 in gas mixtures depends on n-C_4H_{10} concentration, where it exhibits a maximum (12.2 ± 1.5 kJ/mol) at 50 cm^3(STP)/cm^3 n-C_4H_{10}. For comparison, the mixed gas E_D^C of CH_4 in PDMS in the presence of 50 cm^3(STP)/cm^3 n-C_4H_{10} is 12.1 kJ/mol. The increase in CH_4 E_D^C as n-C_4H_{10} concentration increases may be related to the blocking effect by n-C_4H_{10} that hinders CH_4 transport through the polymer. As n-C_4H_{10} competitively

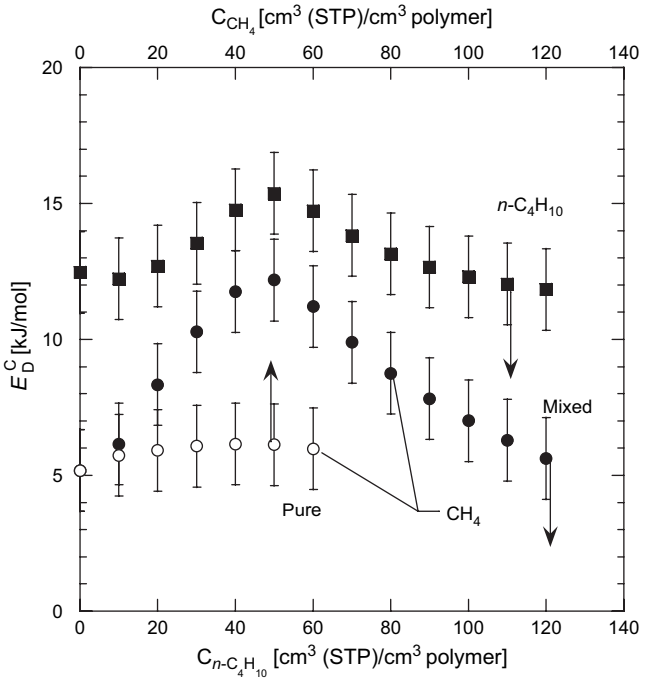

Fig. 9. Pure and mixed gas activation energy of diffusion for CH_4 and n-C_4H_{10} as a function of penetrant concentration in the polymer at the upstream face of the film. The n-C_4H_{10} activation energies of diffusion are estimated based on mixed gas data. There is essentially no difference between the pure and mixed gas n-C_4H_{10} diffusivity data in PTMSP, so the activation energies of diffusion of n-C_4H_{10} are the same, within the uncertainty in the measurements, in both pure and mixed gas cases. The error bars were determined using the propagation of errors method [28].

occupies the more facile permeation pathways, methane transport is restricted to routes requiring more energy. As n-C_4H_{10} concentration increases, the plasticization effect, which enhances CH_4 transport and reduces E_D^C, begins to dominate. This phenomenon is shown in Fig. 9, where the E_D^C of CH_4 decreases with increasing n-C_4H_{10} concentration at high n-C_4H_{10} concentrations. The E_D^C of n-C_4H_{10} also shows a concentration dependence similar to that of the E_D^C of CH_4 in mixture. The E_D^C of n-C_4H_{10} reaches a maximum value of 15.4 ± 1.5 kJ/mol at a n-C_4H_{10} concentration of 50 cm^3(STP)/cm^3. However, the dependence of E_D^C of n-C_4H_{10} on n-C_4H_{10} concentration is weaker than that of CH_4 in gas mixtures.

4.5. Dual mode permeability model

4.5.1. Pure gas

The dual mode permeability model (Eq. (8)) describes the pure gas permeability data reasonably well. The values of k_D, C'_H, and b for CH_4 and n-C_4H_{10} have been reported previously [11]. The best fit $\overline{D}_D$ and $\overline{D}_H$ values for CH_4, determined by plotting experimental pure gas permeability data versus $[(1 + b_A f_{A,2})]^{-1}$, are reported in Table 1. The CH_4 pure gas permeability values calculated using Eq. (8) and the parameters in Table 1 are represented by solid lines in Fig. 1(a). The concentration average diffusion coefficient for gas A, $\overline{D}_A$, is given by the dual mode model as follows [15]:

$$\overline{D}_A = \frac{\overline{D}_{D_A} k_{D_A} + \overline{D}_{H_A} \frac{C'_{H_A} b_A}{1 + b_A f_{A,2}}}{k_{D_A} + \frac{C'_{H_A} b_A}{1 + b_A f_{A,2}}} \tag{22}$$

Values of the concentration-averaged diffusion coefficient according to Eq. (22) for n-C_4H_{10} at pure gas conditions are represented by the lines in Fig. 2(a).

4.5.2. Mixed gas

The dual mode permeability model can be extended to mixtures, as shown in Eqs. (10) and (11). In the remainder of the article, the subscripts A and B correspond to n-C_4H_{10} and CH_4, respectively. This model describes pure and mixed gases' n-C_4H_{10} permeability data reasonably well. The best fit $\overline{D}_D$ and $\overline{D}_H$ values for n-C_4H_{10} were determined by plotting the experimental pure and mixed gas permeability data versus $[(1 + b_A f_{A,2} + b_B f_{B,2})]^{-1}$ and are recorded in Table 1. Values of n-C_4H_{10} pure and mixed gases permeability as calculated by this model using the parameters in Table 1 are the solid lines in Figs. 1(b) and 4. The concentration average diffusion coefficient, $\overline{D}_A$, for n-C_4H_{10} in pure gas and mixtures is given by the dual mode model as follows [16]:

$$\overline{D}_A = \frac{\overline{D}_{D_A} k_{D_A} + \overline{D}_{H_A} \frac{C'_{H_A} b_A}{1 + b_A f_{A,2} + b_B f_{B,2}}}{k_{D_A} + \frac{C'_{H_A} b_A}{1 + b_A f_{A,2} + b_B f_{B,2}}} \tag{23}$$

where the subscripts A and B correspond to n-C_4H_{10} and CH_4, respectively. Calculations according to Eq. (23) are represented as solid lines in Figs. 2(b) and 6(b). Table 1 shows that $\overline{D}_D$ is greater than $\overline{D}_H$, consistent with previous results for PTMSP and glassy polymers in general [3,15]. The local effective diffusion coefficient, D_A, for n-C_4H_{10} can be calculated using the dual mode model as follows [3]:

$$D_A = \frac{\overline{D}_{D_A} k_{D_A} + \overline{D}_{H_A} \frac{C'_{H_A} b_A}{\left(1 + b_A f_{A,2} + b_B f_{B,2}\right)^2}}{k_{D_A} + \frac{C'_{H_A} b_A}{\left(1 + b_A f_{A,2} + b_B f_{B,2}\right)^2}} \tag{24}$$

Despite the reasonable estimates for n-C_4H_{10} permeability data, the mixed gas model cannot predict mixed gas CH_4 permeability data using the pure gas $\overline{D}_D$ and $\overline{D}_H$ of CH_4 recorded in Table 1. In fact, no single set of dual mode diffusion coefficients could fit simultaneously the pure and mixed CH_4 permeability data. This inability of the mixed gas permeability model to account for the changes in permeability of a light gas in PTMSP has been previously recognized [9]. While the model appropriately accounts for competitive sorption effects in mixtures, it does not consider the blocking effect observed in PTMSP. That is, in the original formulation of the model, the CH_4 dual mode diffusion coefficients are not allowed to depend on the concentration of n-C_4H_{10}. To capture this effect, a concentration dependence of $\overline{D}_H$ is introduced in the dual mode mixed gas permeability model using the following empirical relation:

$$\overline{D}_{H_B} = \overline{D}_{Ho_B} \exp(-\alpha_H \overline{C}_{H_A}) \tag{25}$$

where the subscripts A and B correspond to n-C_4H_{10} and CH_4, respectively, $\overline{D}_{Ho_B}$ is the CH_4 diffusion coefficient in Langmuir region at infinite dilution, α_H is a parameter that quantifies the blocking effect in the Langmuir region induced by the condensable n-C_4H_{10} molecules, and $\overline{C}_{H_A}$ is the average n-C_4H_{10} concentration in the Langmuir region, defined as:

$$\overline{C}_{H_A} = \frac{C'_{H_A} b_A f_{A,2}}{2\left(1 + b_A f_{A,2} + b_B f_{B,2}\right)} \tag{26}$$

The blocking effect is a consequence of the high level of n-C_4H_{10} sorption in the larger free volume elements in the polymer (*i.e.*, Langmuir region) [4]. As such, the decrease in CH_4 mixed gas diffusion coefficients is only attributed to the n-C_4H_{10} concentration in the Langmuir region, as shown in Eq. (25).

Substituting Eq. (25) into Eq. (11) yields a modified dual mode mixed gas permeability model for CH_4:

$$P_B = k_{D_B} \overline{D}_{D_B} + \frac{C'_{H_B} b_B \overline{D}_{Ho_B} \exp(-\alpha_H \overline{C}_{H_A})}{1 + b_A f_{A,2} + b_B f_{B,2}} \tag{27}$$

Eq. (27) captures both the competitive sorption effect and the blocking effect in CH_4 mixture permeation in PTMSP and describes the pure and mixed gases' CH_4 permeability data reasonably well. The best fit $\overline{D}_D$, $\overline{D}_H$, and α_H of CH_4 based on pure and mixed gas data are recorded in Table 2. Permeability coefficients calculated according to Eq. (27) using the parameters from Table 2 are represented by solid lines in Fig. 3(a). The $\overline{D}_D$

of CH_4 obtained from Eq. (27) (Table 2) is an order of magnitude less than that determined from the pure gas measurements (Table 1). The α_H values increase with decreasing temperature; the $\overline{D}_D$ and $\overline{D}_H$ values increase as temperature increases. A linear concentration dependence of $\overline{D}_{H_B}$ (*i.e.*, $\overline{D}_{H_B} = \overline{D}_{Ho_B}(1 - \alpha_H \overline{C}_{H_A})$) could also describe the permeability data as well, but the best fit parameters determined this way lead to negative $\overline{D}_{H_B}$ values, which are physically unrealistic. Theoretically, one might also consider the plasticization effect of the Henry's law region in Eq. (27) by introducing a concentration dependent $\overline{D}_D$ (*i.e.*, $\overline{D}_{D_B} = \overline{D}_{Do_B} \exp(\alpha_D \overline{C}_{D_A})$) [3]. However, when fitting the experimental data to such a model, it is difficult to obtain unique values for α_D, the plasticization parameter, because the plasticization effect is weak relative to the blocking effect. That is, the plasticization effect is not very apparent from Figs. 3(a) and 6(a). The expression for $\overline{D}_B$ according to the modified dual mode permeability model (Eq. (27)) is:

$$\overline{D}_B = \frac{\overline{D}_{D_B} k_{D_B} + \overline{D}_{Ho_B} \exp(-\alpha_H \overline{C}_{H_A}) \frac{C'_{H_B} b_B}{1 + b_A f_{A,2} + b_B f_{B,2}}}{k_{D_B} + \frac{C'_{H_B} b_B}{1 + b_A f_{A,2} + b_B f_{B,2}}} \quad (28)$$

A comparison of calculations according to Eq. (28) and experimental data is shown in Fig. 6(a).

Table 2 shows $\overline{D}_H$ values that are greater than $\overline{D}_D$ values. This result is in contrast to the usual trend in glassy polymers, where $\overline{D}_D$ is usually greater than $\overline{D}_H$ [3,15]. The source of the discrepancy is not known at this time. Another unexplained trend found in this study is the similarity between the $\overline{D}_D$ values in PTMSP for CH_4 from the mixture data (Table 2) and *n*-C_4H_{10} (Table 1), despite the fact that CH_4 is smaller than *n*-C_4H_{10}, so one would anticipate that its diffusion coefficients would be larger. Nevertheless, this model provides a convenient mathematical expression for gas and vapor permeation in PTMSP.

Gas diffusivity is often correlated with the amount of fractional free volume (FFV) in the polymer [34,35]. Gas diffusivity commonly increases as the amount of FFV in the polymer increases [15]. Fig. 10 presents the CH_4 effective diffusion coefficients in pure gas and mixtures in PTMSP, at various *n*-C_4H_{10} and CH_4 concentrations and temperatures, as a function of inverse local FFV in the polymer/penetrant mixture. The local FFV values were estimated from the experimental sorption and dilation data in PTMSP [11], as described previously [21]. Fig. 10 shows no distinct trend in diffusion coefficients with FFV in PTMSP. Part of the trend actually shows an increase in CH_4 diffusion coefficients with decreasing FFV. The reasons for this lack of coherence with the free volume model are not immediately known, in part due to a lack of similar literature data (*i.e.*, where FFV in the polymer/penetrant mixture is estimated based on experimental data). In our previous mixture study in PDMS, the effective diffusion coefficients of CH_4 and *n*-C_4H_{10} increase as the FFV in the polymer/penetrant mixture increases [21]. Although further study of this phenomenon may result a better understanding of the relationship between gas diffusivity and FFV in the polymer, it appears that FFV is not the only factor contributing

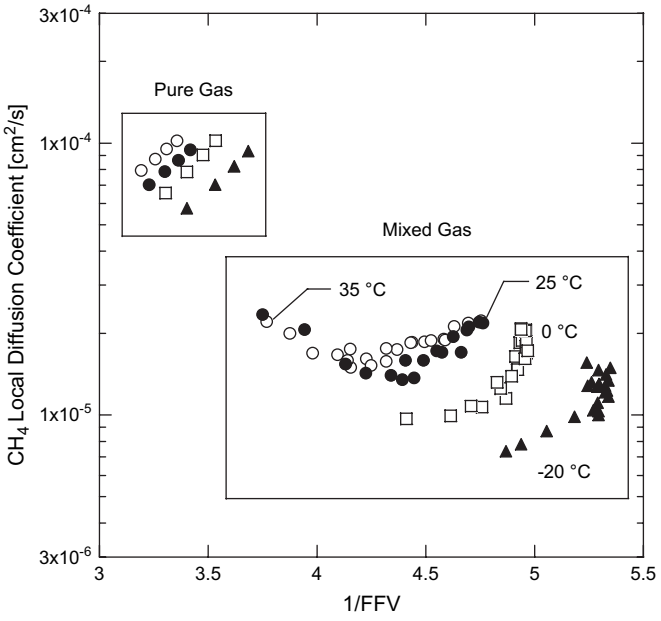

Fig. 10. Correlation between fractional free volume of the polymer/penetrant mixtures and effective diffusion coefficients of CH_4 in PTMSP at various penetrant concentrations and temperatures. The FFV was estimated based on penetrant concentrations at the upstream face of the film as described in Ref. [21].

to the temperature and concentration dependence of diffusion coefficients in PTMSP.

A key question regarding the permeation properties of PTMSP has been whether the primary mechanism is via preferential sorption or surface diffusion along the walls of interconnected free volume elements (or pores) in this very high free volume polymer. Srinivasan et al. and Pinnau and Toy suggested that this was the case [4,9]. Additionally, Singh found rather compelling evidence that PTMSP is, in fact, a "borderline" material between conventional, dense, low free volume polymers and microporous materials such as microporous carbon [36]. Singh's studies compared the gas diffusion coefficients calculated from transient kinetic uptake experiments with those estimated from steady state permeability and sorption measurements, similar to the techniques used in this manuscript. Order of magnitude differences were observed in the diffusion coefficients estimated by these two methods, clearly suggesting that most of the gas transport in PTMSP was through interconnected free volume elements or "pores" inherently present in the material due, presumably, to its intrinsically high free volume and unusual distribution of free volume [37,38]. However, the models and data analysis considered in this study can be applied to both microporous and nonporous materials. Thus, while the data presented in this study do not definitively prove that the dominant mechanism for gas and vapor transport in PTMSP occurs via micropore transport, they are consistent with such an interpretation.

4.6. Selectivity

Fig. 11(a) presents mixed gas *n*-C_4H_{10}/CH_4 permeability selectivity in PTMSP as a function of *n*-C_4H_{10} upstream

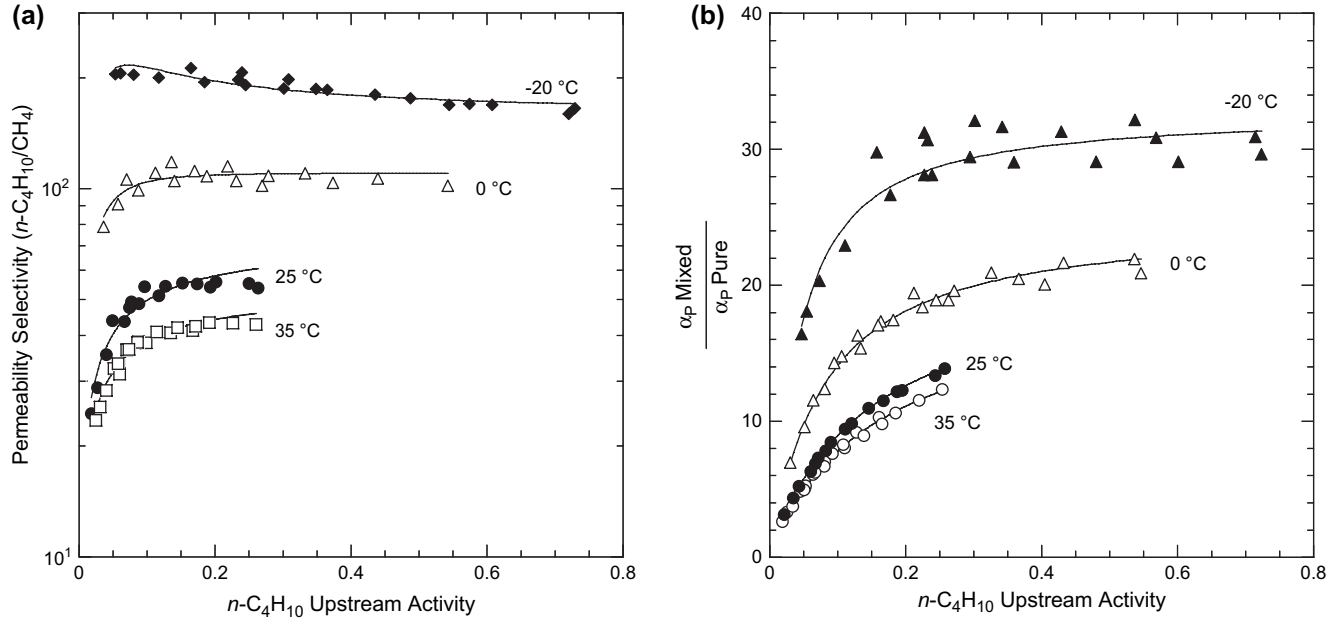

Fig. 11. (a) Mixed gas n-C_4H_{10}/CH_4 permeability selectivity in PTMSP as a function of n-C_4H_{10} upstream activity. (b) Ratio of n-C_4H_{10}/CH_4 mixed gas to pure gas permeability selectivity in PTMSP. The pure gas permeability selectivity is calculated from n-C_4H_{10} permeability at different n-C_4H_{10} upstream activity values and CH_4 pure gas permeability at infinite dilution. The lines represent predictions of the dual mode mixture permeability model (*i.e.*, Eqs. (8) and (27)).

activity in the mixtures. At low n-C_4H_{10} activity, the permeability selectivity increases with increasing n-C_4H_{10} activity. For example, at 25 °C, n-C_4H_{10}/CH_4 mixed gas permeability selectivity increases two-fold from 25 to 51, as n-C_4H_{10} upstream activity increases from 0.02 to 0.11. At higher n-C_4H_{10} activity (>0.1), the permeability selectivity apparently reaches a plateau. The permeability selectivity increases with decreasing temperature: *e.g.*, the n-C_4H_{10}/CH_4 mixed gas permeability selectivity at 0.22 n-C_4H_{10} upstream activity increases from 43 to 197 as temperature decreases from 35 to −20 °C. Fig. 11(b) presents the ratio of the n-C_4H_{10}/CH_4 mixed gas to pure gas permeability selectivity at various temperatures. Due to CH_4 permeability depression in the mixture, the permeability selectivities determined from the mixture measurements are considerably higher than those estimated from pure gas data. These differences between the pure and mixed gas permeability selectivities are even greater at higher n-C_4H_{10} activity and lower temperature. For example,

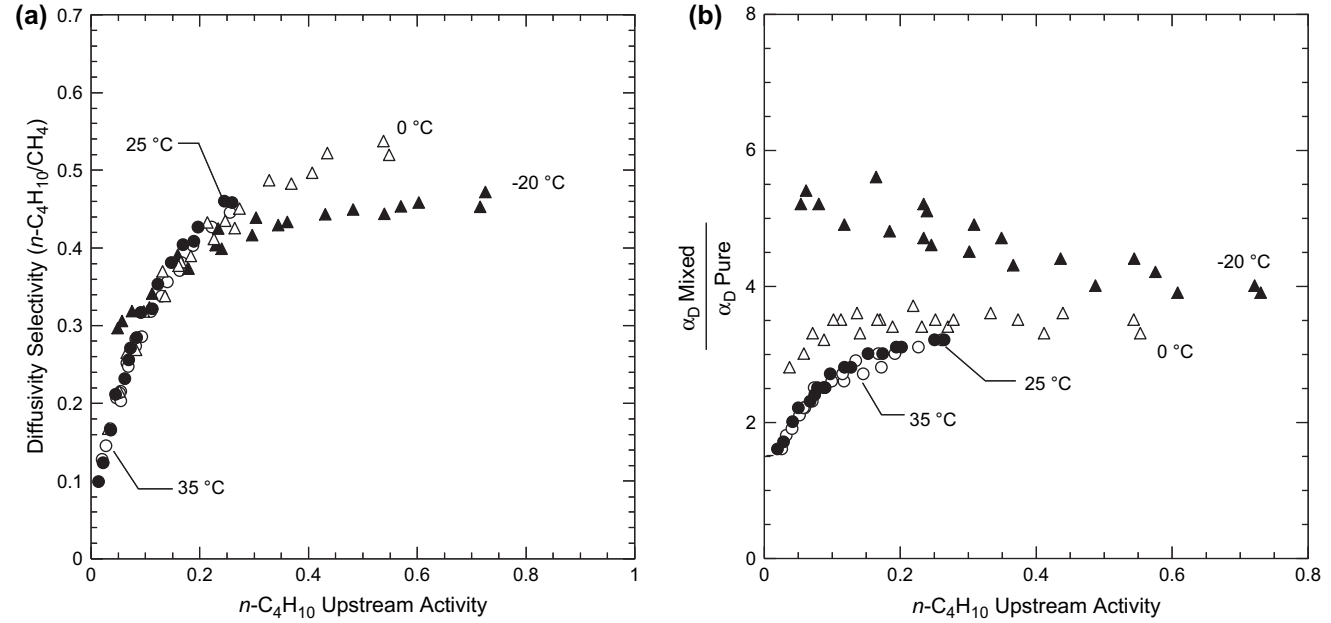

Fig. 12. (a) Mixed gas n-C_4H_{10}/CH_4 diffusivity selectivity in PTMSP as a function of n-C_4H_{10} upstream activity. (b) Ratio of n-C_4H_{10}/CH_4 mixed gas to pure gas diffusivity selectivity in PTMSP. The pure gas diffusivity selectivity is calculated from n-C_4H_{10} diffusivity values at the indicated n-C_4H_{10} upstream activity values and CH_4 pure gas diffusivity at infinite dilution.

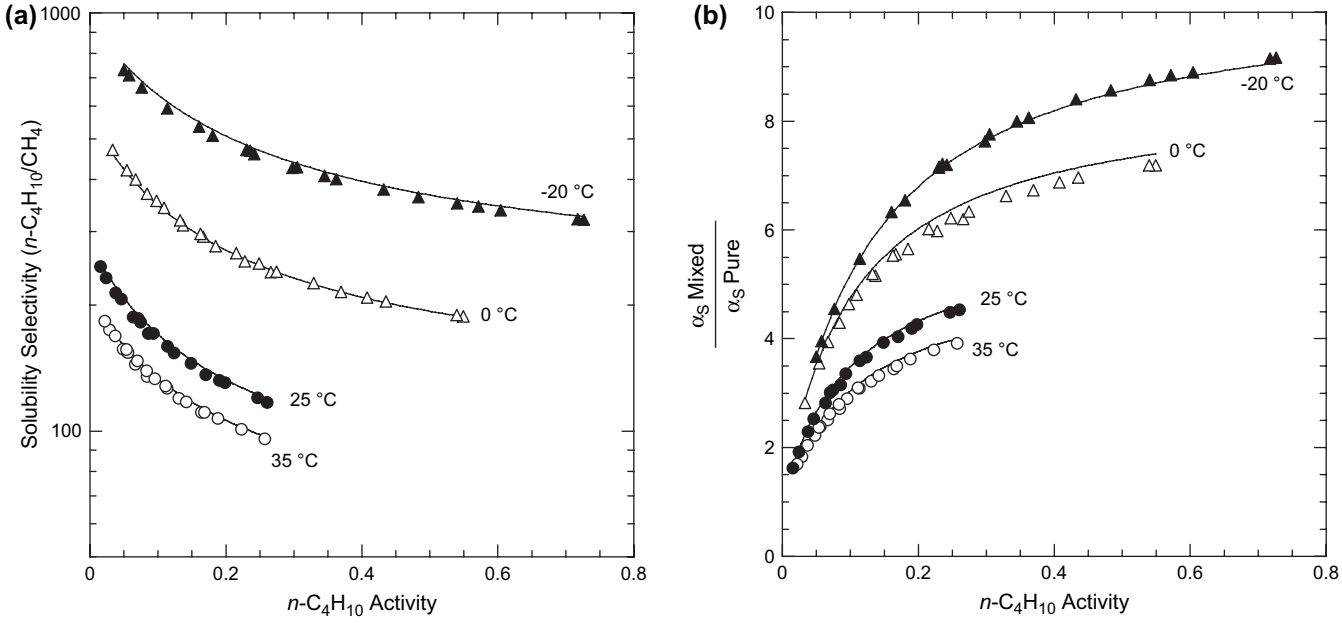

Fig. 13. (a) Mixed gas n-C_4H_{10}/CH_4 solubility selectivity in PTMSP as a function of n-C_4H_{10} activity in the mixture. (b) Ratio of n-C_4H_{10}/CH_4 mixed gas to pure gas solubility selectivity in PTMSP. The pure gas solubility selectivity is calculated from n-C_4H_{10} pure gas solubility at the indicated n-C_4H_{10} activity values and CH_4 pure gas solubility in the limit of zero CH_4 fugacity. The lines represent predictions of the dual mode sorption model [11]. These figures were reprinted from Ref. [11], Copyright Elsevier (2007).

at 0 °C and 0.54 n-C_4H_{10} upstream activity, the mixed gas permeability selectivity is approximately 22 times higher than the pure gas selectivity.

Fig. 12(a) presents n-C_4H_{10}/CH_4 mixed gas diffusivity selectivity in PTMSP as a function of n-C_4H_{10} upstream activity and temperature. The diffusivity selectivity increases with increasing n-C_4H_{10} activity. For example, at 0 °C, the diffusivity selectivity increases from 0.17 to 0.54 as n-C_4H_{10} upstream activity increases from 0.03 to 0.54. This trend is observed in part due to the decrease in CH_4 diffusion coefficient when n-C_4H_{10} is present in the mixture (*i.e.*, the blocking effect). The n-C_4H_{10} diffusion coefficients also increase with increasing n-C_4H_{10} upstream activity. Interestingly, this trend is relatively insensitive to temperature. The diffusivity selectivity data at various temperatures, in general, nearly fall on a single master curve. The n-C_4H_{10}/CH_4 diffusivity selectivities in PTMSP determined in this study are between 0.15 and 0.54. Fig. 12(b) presents the ratio of the n-C_4H_{10}/CH_4 mixed gas to pure gas diffusivity selectivity at various temperatures. The diffusivity selectivities determined from the mixed gas measurements are higher than those estimated from the pure gas data, due to the blocking effect that considerably reduces CH_4 diffusion coefficient in mixtures. With the exception of the data at −20 °C, the difference between mixed gas and pure gas diffusivity selectivities generally increases with increasing n-C_4H_{10} upstream activity. As indicated in Fig. 6(a), the CH_4 diffusivity at −20 °C increases modestly at n-C_4H_{10} activities greater than approximately 0.05, presumably due to plasticization of the polymer by n-C_4H_{10}. This increase in mixed gas CH_4 diffusion coefficients at −20 °C causes the decrease in the diffusivity selectivity ratio observed at −20 °C in Fig. 12(b).

Based on our mixed gas sorption study in PTMSP [11], the n-C_4H_{10}/CH_4 mixed gas solubility selectivity in PTMSP decreases with increasing n-C_4H_{10} activity and temperature, as shown in Fig. 13(a), because n-C_4H_{10} solubility decreases more than CH_4 solubility with increasing n-C_4H_{10} activity. For instance, at −20 °C, the n-C_4H_{10}/CH_4 mixed gas solubility selectivity decreases from 690 to 480 as n-C_4H_{10} activity increases from 0.05 to 0.24. At 35 °C, the solubility selectivity

Table 3
Effect of temperature on pure and mixed gases' n-C_4H_{10}/CH_4 permeability, solubility, and diffusivity selectivities

T (°C)	Permeability selectivity			Solubility selectivity			Diffusivity selectivity		
	Mixed[a]	Pure[b]	Mixed/pure	Mixed[a]	Pure[b]	Mixed/pure	Mixed[a]	Pure[b]	Mixed/pure
−20	167 ± 8	5.2 ± 0.3	32 ± 2	351 ± 18	40 ± 2	8.8 ± 0.4	0.48 ± 0.05	0.11 ± 0.01	4.4 ± 0.5
0	109 ± 5	5.7 ± 0.3	19 ± 1	251 ± 13	40 ± 2	6.2 ± 0.3	0.43 ± 0.04	0.13 ± 0.01	3.5 ± 0.4
25	51 ± 3	5.4 ± 0.3	9.5 ± 0.6	159 ± 8	44 ± 2	3.6 ± 0.2	0.32 ± 0.03	0.12 ± 0.01	2.8 ± 0.3
35	38 ± 2	5.6 ± 0.3	6.8 ± 0.4	139 ± 7	50 ± 3	2.8 ± 0.1	0.27 ± 0.03	0.11 ± 0.01	2.5 ± 0.3

[a] Feed composition: 6 mol% n-C_4H_{10}; feed pressure: 4.4 atm. The permeate side of the film was swept with helium.
[b] Estimated using n-C_4H_{10} mixture properties at the upstream conditions as specified in table footnote "a" and CH_4 pure gas properties at infinite dilution from Table 1 and Ref. [11].

decreases from 175 to 96 as n-C_4H_{10} activity increases from 0.03 to 0.26. As shown in Fig. 13(b), the solubility selectivities determined from the mixed gas measurements are considerably higher than those estimated from pure gas data, due to the competitive sorption effect, which decreases CH_4 solubility in the mixture [11]. These differences between pure and mixed solubility selectivities are even greater at higher n-C_4H_{10} activity and lower temperature.

Table 3 compares pure and mixed gases n-C_4H_{10}/CH_4 permeability, solubility, and diffusivity selectivities at various temperatures. As shown in Fig. 11(b), the permeability selectivities determined from mixed gas measurements are higher than those estimated from pure gas data. The difference is a result of both higher solubility and diffusivity selectivity in mixtures relative to those in pure gas. Table 3 presents the ratios of the mixed gas selectivities to those of pure gas. The mixed gas permeability selectivity at 35 °C is 6.8 times higher than that estimated from pure gas measurements, and the deviation is greater at lower temperatures: at −20 °C, the mixed gas permeability selectivity is 32 times higher than the pure gas values. At this temperature, the solubility and diffusivity selectivities are 8.8 and 4.4 times, respectively, higher than their pure gas values.

5. Conclusions

Although n-C_4H_{10} transport properties are essentially unaffected by the presence of CH_4, CH_4 permeability in PTMSP is considerably reduced by the presence of n-C_4H_{10}. This depression in CH_4 permeability arises from competitive sorption, which reduces CH_4 solubility in mixtures, and from blocking, which reduces CH_4 diffusivity in mixtures. The mixed gas CH_4 permeability data can be predicted using a modified dual mode mixture permeability model. The n-C_4H_{10}/CH_4 permeability selectivity increases with increasing n-C_4H_{10} upstream activity and decreasing temperature due to the competitive sorption and blocking effects, both of which favor n-C_4H_{10} permeation over that of CH_4. The n-C_4H_{10}/CH_4 diffusivity selectivity also increases with increasing n-C_4H_{10} upstream activity, but it is a weak function of temperature. On the other hand, the n-C_4H_{10}/CH_4 solubility selectivity decreases with increasing n-C_4H_{10} activity and temperature. The difference between the n-C_4H_{10}/CH_4 permeability selectivity in pure gas and mixtures in PTMSP is due to both solubility and diffusivity effects.

Acknowledgement

We gratefully acknowledge partial support of this work by the U.S. Department of Energy (DE-FG03-02ER15362) and the National Science Foundation (CTS-0515425).

Appendix. Supplementary section

Supplementary data associated with this article can be found, in the online version at, doi:10.1016/j.polymer.2007.10.024.

References

[1] Baker RW. Membrane technology and applications. 2nd ed. New York: John Wiley & Sons; 2004.
[2] Merkel TC, Bondar VI, Nagai K, Freeman BD, Pinnau I. Journal of Polymer Science Part B: Polymer Physics 2000;38:415–34.
[3] Merkel TC, Bondar V, Nagai K, Freeman BD. Journal of Polymer Science Part B: Polymer Physics 2000;38:273–96.
[4] Pinnau I, Toy LG. Journal of Membrane Science 1996;116:199–209.
[5] Pinnau I, Casillas CG, Morisato A, Freeman BD. Journal of Polymer Science Part B: Polymer Physics 1996;34:2613–21.
[6] Morisato A, Freeman BD, Pinnau I, Casillas CG. Journal of Polymer Science Part B: Polymer Physics 1996;34:1925–34.
[7] Pope DS, Koros WJ, Hopfenberg HB. Macromolecules 1994;27:5839–44.
[8] Ghisellini M, Quinzi M, Giacinti Baschetti M, Doghieri F, Costa G, Sarti GC. Desalination 2002;149:441–5.
[9] Srinivasan R, Auvil SR, Burban PM. Journal of Membrane Science 1994;86:67–86.
[10] Rojey A, Jaffret C, Cornot-Gandolphe S, Durand B, Jullian S, Valais M. Natural gas production processing transport. Paris: Editions Technip; 1997.
[11] Raharjo RD, Freeman BD, Sanders ES. Polymer 2007;48:6097–114.
[12] Matteucci S, Yampolskii Y, Freeman BD, Pinnau I. Transport of gases and vapors in glassy and rubbery polymers. In: Yampolskii Y, Pinnau I, Freeman BD, editors. Materials science of membranes. Chichester: John Wiley & Sons, Ltd.; 2006.
[13] Raharjo RD, Freeman BD, Sanders ES. Journal of Membrane Science 2007;292:45–61.
[14] Paul DR. Journal of Membrane Science 2004;241:371–86.
[15] Ghosal K, Freeman BD. Polymers for Advanced Technologies 1994;5:673–97.
[16] Koros WJ, Chern RT, Stannett V, Hopfenberg HB. Journal of Polymer Science Part B: Polymer Physics 1981;19:1513–30.
[17] Prabhakar RS, Raharjo R, Toy LG, Lin H, Freeman BD. Industrial & Engineering Chemistry Research 2005;44:1547–56.
[18] Nagai K, Nakagawa T. Journal of Membrane Science 1995;105:261–72.
[19] Stern SA, Gareis PJ, Sinclair TF, Mohr PH. Journal of Applied Polymer Science 1963;7:2035–51.
[20] O'Brien KC, Koros WJ, Barbari TA. Journal of Membrane Science 1986;29:229–38.
[21] Raharjo RD, Freeman BD, Paul DR, Sarti GC, Sanders ES. Journal of Membrane Science 2007;306:75–92.
[22] Poling BE, Prausnitz JM, O'Connell JP. The properties of gases and liquids. 5th ed. New York, NY: McGraw-Hill; 2001.
[23] Raharjo RD, Lee HJ, Freeman BD, Sakaguchi T, Masuda T. Polymer 2005;46:6316–24.
[24] Ichiraku Y, Stern SA, Nakagawa T. Journal of Membrane Science 1987;34:5–18.
[25] Nagai K, Masuda T, Nakagawa T, Freeman BD, Pinnau I. Progress in Polymer Science 2001;26:721–98.
[26] Hu Y, Shiotsuki M, Sanda F, Masuda T. Chemical Communications 2007;41:4269–70.
[27] Koros WJ, Chan AH, Paul DR. Journal of Membrane Science 1977;2:165–90.
[28] Bevington PR. Data reduction and error analysis for the physical sciences. 3rd ed. New York, NY: McGraw-Hill; 2002.
[29] Masuda T, Iguchi Y, Tang B-Z, Higashimura T. Polymer 1988;29:2041–9.
[30] Merkel TC, He Z, Pinnau I, Freeman BD, Meakin P, Hill AJ. Macromolecules 2003;36:6844–55.
[31] Pauly S. Permeability and diffusion data. In: Brandrup J, Immergut EH, Grulke EA, editors. Polymer handbook. Toronto: John Wiley & Sons, Ltd.; 1999.
[32] Koros WJ, Hellums MW. Transport properties. In: Kroschwitz JI, editor. Encyclopedia of polymer science and technology. New York: Wiley; 1990. p. 724–802.
[33] Koros WJ, Paul DR. Journal of Polymer Science Polymer Physics Edition 1978;16:2171–87.

[34] Cohen MH, Turnbull D. Journal of Chemical Physics 1952;31: 1164–9.
[35] Lee WM. Polymer Engineering and Science 1980;20:65–9.
[36] Singh A. Ph.D. dissertation, North Carolina State University; 1997.
[37] Shantarovich VP, Kevdina IB, Yampolskii YP, Alentiev AY. Macromolecules 2000;33:7453–66.
[38] Hill AJ, Freeman BD, Jaffe M, Merkel TC, Pinnau I. Journal of Molecular Structure 2005;739:173–8.